11th International Symposium on Turbulence and Shear Flow Phenomena (TSFP11)
Southampton, UK, July 30 to August 2, 2019

2D ROUGHNESS EFFECTS ON CROSSFLOW INSTABILITIES

T. I. Saeed
Department of Aeronautics
Imperial College London
South Kensington, SW7 2AZ
t.saeed@cantab.net

J. F. Morrison
Department of Aeronautics
Imperial College London
South Kensington, SW7 2AZ
j.morrison@imperial.ac.uk

ABSTRACT

A crossflow transition experiment is performed for a 40° swept-back wing with moderate free-stream turbulence, $Tu = 0.13\%$, at $Re_c \simeq 1 \times 10^6$. Periodic Discrete Roughness Elements (DRE), spaced at the critical crossflow wavelength, are used to excite the crossflow disturbance. The subsequent interaction with a 2D roughness strip of variable height and chordwise location is investigated through boundary-layer hot-wire measurements.

When the 2D roughness is located near the neutral point, stationary crossflow amplification is observed for strip heights up to 80% of δ_{99}, above which it is attenuated. Thereafter, the unsteady disturbances are rich in high-frequency fluctuations, similar to those reported for a backward facing step. Moving the strip downstream results in a lower critical roughness height and earlier transition. In the absence of DRE forcing, a strip located near the neutral point amplifies the stationary crossflow, selecting the critical crossflow wavelength, albeit at a much lower amplitude.

BACKGROUND

Recent publications have provided much insight into the role that 2D roughness plays in crossflow transition (Duncan Jr. *et al.*, 2013; Duncan Jr *et al.*, 2014; Crawford *et al.*, 2015; Tufts *et al.*, 2017; Eppink *et al.*, 2018). All of these have investigated the effects of forward and backward facing steps in isolation. Forward facing steps were shown to amplify the stationary crossflow disturbance, while backward facing steps introduced unsteadiness that could be attributed to both 2D and 3D instabilities. However, there is further scope for exploring the influence of 2D roughness in the form of strips that feature both forward and backward facing steps. Having established a crossflow-dominated boundary layer and quantified both the stationary and travelling-wave disturbances in the first part of this experiment, we seek to explore the interaction of a 2D roughness strip with crossflow disturbances, and determine whether the insights from studying the effects of backward and forward facing steps in isolation are still relevant to the practical problem of a 2D strip. Our objectives are to quantify the sensitivity of the response to strip height and location, primarily in terms of the evolution of both stationary and travelling-wave crossflows.

EXPERIMENTAL SETUP

Experiments were performed in a closed-loop facility with a working section of 2.3 m x 1.8 m x 6.0 m for flow speeds of up to 48 m/s. The tunnel has a contraction ratio of 8:1 with one honeycomb, one curved screen in the rapid-diffuser located upstream of the contraction, and two turbulence-reducing screens. The tunnel does not have active temperature control, but velocity feedback is used to control the free-stream velocity U_∞ and maintain a constant Reynolds number $Re_c \simeq 1 \times 10^6$. A side view of the experimental setup is shown in Figure 1.

The "AERAST" swept wing model was provided by Airbus (Sunderland & Sawyers, 2009). It has a sweep angle $\Lambda = 40°$, and a leading-edge radius and ellipse aspect ratio combination to avoid attachment-line instability. The constant section chord, $c = 0.8$ m and span, $b = 1.2$ m. The model is constructed from aluminium and has streamwise rows of pressure ports, each with 49 tappings, at three spanwise, z/b, locations: 25%, 50% and 75% span. The leading 10% of chord on the suction surface (the test side) is hand-polished to a surface finish of 0.06 μm rms. The wing root incidence is $-2.15°$, with a tip-down linear twist of 1.5°.

The model was mounted vertically on the tunnel floor, incorporating a boundary-layer splitter plate to avoid turbulence contamination along the leading edge. Boundary layer measurements were conducted using hot-wire anemometry and consisted of spanwise scans across the boundary layer at a constant x/c, and spanning a minimum of three crossflow vortex wavelengths. The minimum traverse step size in the spanwise (parallel to the leading edge) and wall-normal directions were $\Delta z = 2.5$ μm and $\Delta Y = 2.5$ μm, respectively.

To ensure the generation of crossflow disturbances, an array of Discrete Roughness Elements (DREs), was placed around the neutral point. These were produced by appliqué roughness elements printed on a dry-ink transfer sheet, with

a wavelength, $\lambda_c = 8.4$ mm; the optimal element diameter for the excitation of the most critical stationary crossflow wave was calculated to be $d = 3.4$ mm, using a linearised Navier-Stokes method (Mughal & Ashworth, 2013). The elements were placed close to the neutral point $x_{NP}/c = 0.02$, and applied over 50% of the model span (with the measurement region located between 25% – 50% span). The 2D roughness strip was placed downstream of the DREs. It consists of superimposed layers of $w = 3$ mm wide strips of Kapton tape, with each layer of height, $h = 55$ μm. For this study, a DRE height of $k = 44$ μm was used as a baseline. The strip height is $110 \leq h \leq 660$ μm located at $x_h/c = 0.03$, 0.10, and 0.20. Here, we refer to cases corresponding to $h = (495, 660)$ μm as h_{495} and h_{660}, respectively.

DATA ANALYSIS

The stationary crossflow disturbance amplitude is quantified by the method of Downs (2012). (See also Bippes, 1999). The spanwise r.m.s of the steady disturbance profiles, U'_{rms}, represents the stationary crossflow mode shape, and is given by:

$$U'_{rms}(Y) = \sqrt{\frac{1}{n}\sum_{j=0}^{n-1}\left(\bar{U}(Y) - U(Y,z_j)\right)^2}, \qquad (1)$$

where $\bar{U}(Y)$ is the spanwise-averaged velocity profile, $U(Y,z_j)$ is the velocity profile at a particular spanwise location, and n is the total number of spanwise profiles – as is common, all velocity profiles are normalised by U_e. Wavenumber spectra are determined by calculating the power spectral density of $U'_{rms}|_{Y_{max}}(z)$.

The stationary mode disturbance amplitude is given by

$$A = \frac{1}{\delta_{99.9}}\int_0^{\delta_{99.9}} U'_{rms}(Y)\,\mathrm{d}Y, \qquad (2)$$

where $\delta_{99.9}$ is the height of the $\bar{U}(Y)$ profile at 99.9% velocity ratio. The streamwise fluctuation intensity is given by

$$|u'_{rms}(Y)|_z = \frac{1}{z_{max}}\int_0^{z_{max}} u'_{rms}(Y,z)\,\mathrm{d}z, \qquad (3)$$

where z_{max} is the extent of the spanwise measurement domain. The unsteady disturbance amplitude is then calculated in a similar manner to the stationary disturbance amplitude:

$$a = \frac{1}{\delta_{99.9}}\int_0^{\delta_{99.9}} |u'_{rms}(Y)|_z\,\mathrm{d}Y. \qquad (4)$$

Coherence, $\gamma(f)$, is a useful measure of the relationship between two time series as a function of frequency (Eppink, 2014),

$$\gamma(f) = \frac{|S_{12}(f)|^2}{S_{11}(f)S_{22}(f)}, \qquad (5)$$

where the auto and cross-spectral densities are, respectively, S_{11}, S_{22} and S_{12} and subscripts '1' and '2' correspond to wires 1 and 2 respectively.

RESULTS & DISCUSSION

Disturbance amplitudes from boundary-layer measurements at $x/c = 0.25$, detailing the influence of strip height and chordwise location is shown in Figure 2. The stationary crossflow amplitude increases significantly for $h \leq 495$ μm, when located close to the neutral point at $x_h/c = 0.03$ – here, $h_{495}/\delta_{99\%} \approx 0.61$. A further increase of strip height, $h = 660$ μm ($h_{660}/\delta_{99\%} \approx 0.81$), shows a drop in stationary disturbance amplitude (below undisturbed levels) without resulting in an immediate upstream movement of the transition location to the strip location (as observed by Duncan Jr. *et al.* (2013); Duncan Jr *et al.* (2014); Crawford *et al.* (2015) for forward facing steps). The two downstream locations also show a rise in disturbance amplitude, but at a much lower rate, reaching progressively lower values as the strip is moved downstream. For $x_h/c = 0.10$, the disturbance amplitude reaches a plateau. The unsteady counterpart increases for measurements with the strip at $x_h/c = 0.03$, plateauing for $h > 495$ μm. With the strip positioned at $x_h/c = 0.10, 0.20$, the effect on a is much reduced, similar to that observed for A. We note that the flow is turbulent for $h > 615$ μm at $x_h/c = 0.03, 0.10$, and $h > 495$ μm for $x_h/c = 0.20$. Two observations have been made that warrant further investigation: 1) with the strip near the neutral point at $x_h/c = 0.03$, an increase in strip height amplifies the stationary crossflow, and to a lesser extent the travelling-wave crossflow; 2) downstream translation of the strip produced a less amplified crossflow disturbance at the measurement location, but results in transition at a lower strip height.

Influence of strip height near neutral point

Figure 3 details the evolution of the stationary and travelling-wave crossflow disturbances, respectively, for $x_h/c = 0.03$. The initial amplitude of stationary disturbances is seen to increase up to h_{495}, above which there is little difference from the undisturbed case. In contrast, there is a sharp increase in unsteady disturbance amplitude from h_{495} to h_{660}. The subsequent growth of both stationary and unsteady crossflow disturbances is unaffected by the roughness strip up to h_{495}. At h_{660} there is, however, a sharp reduction in the growth rate of both disturbance types, well below undisturbed values. This suggests that, for large strip heights (greater than 80% of the boundary layer thickness) crossflow disturbances are attenuated, with growth rates deviating significantly from those predicted by linear stability theory.

Figure 4 shows mean and fluctuating velocity contour plots for h_{495} and h_{660}, measured at $x/c = 0.15$. The stationary crossflow continues to evolve for h_{495}, primarily at the critical crossflow wavelength, but is attenuated for h_{660}. A snapshot of U and u' at $x/c = 0.25$ is provided in Figure 5, which shows that, while the stationary crossflow continues to develop for h_{495}, no obvious stationary crossflow structure emerges for h_{660}. There are periodic, and distinctly separate, areas of high fluctuating velocity that coincide with regions of high $\mathrm{d}U/\mathrm{d}z$. As the strip height is increased, the fluctuating velocity intensity increases in magnitude, and neighbouring regions of high intensity merge. Once the stationary crossflow structure is lost for h_{660}, the fluctuating velocities become more uniformly distributed.

Figure 6 shows the PSD of u' at $x/c = 0.15$ and 0.25. At both chordwise locations, there is little difference between the case where there is no strip and h_{495}. For the largest roughness height, the spectra are rich in high frequency unsteadiness with distinct peaks at 430 Hz, 860 Hz and 1290

Hz. Such characteristics of the unsteady signal were observed by Eppink *et al.* (2018), who studied the effects of a backward facing step and attributed these disturbances to: a travelling-wave crossflow, a T-S wave and a shear-layer instability, in that order of increasing frequency.

Measurements were repeated at $x/c = 0.25$ with the strip at $x_h/c = 0.03$ in the absence of critical spaced forcing DRE array. A periodogram of the stationary crossflow disturbance velocity U' is shown in Figure 7(a). It shows that the presence of the strip for h_{495} does excite stationary crossflow disturbances, and naturally picks out the critical crossflow wavelength at $\lambda_c = 8.4$ mm and its associated harmonics. This observation is in contrast to those of Deyhle & Bippes (1996) who reported no modification of the mean disturbance profile; albeit, the disturbance amplitude is an order of magnitude lower than that due to a spanwise array of DREs. Power spectral densities of the streamwise velocity fluctuation u' is shown in Figure 7(b). The clean leading-edge case shows two distinct peaks at: $f \approx 300$ Hz, associated with the travelling crossflow waves; and $f \approx 800$ Hz ($F = 2\pi f \nu / U_\infty^2 \simeq 195$), with T-S waves. Introduction of the strip for h_{495} excites disturbances at frequencies $f < 300$ Hz. Increase of the strip height to h_{660} causes the power spectral distribution to be altered significantly, with disturbances in the range 100 Hz – 1000 Hz up to $\mathcal{O}(10^4)$ higher. The area under the pre-multipied spectrum (insert) shows that the highest energy modes are between 100 Hz – 500 Hz. This coincides with the range of critical travelling-wave frequencies.

Influence of strip location

The spectra of spanwise stationary disturbances and streamwise fluctuating velocities are provided in Figure 8. The stationary crossflow disturbance is most amplified for h_{495} at $x_h/c = 0.03$ at the critical wavelength and its harmonics. As the 2D strip is moved downstream, the amplitude reduces, while it appears that there is a shift of the critical wavelength to a higher value with the strip place at $x_h/c = 0.20$ — here, $h_{495}/\delta_{99\%} \approx 0.28$. Measurements for h_{495} show broadband amplification of unsteady disturbances in the range 300 Hz – 2000 Hz. From this we draw the conclusion that strips located further downstream, interacting with more amplified crossflow disturbances, have a lower critical roughness height with transition brought about through amplification of unsteady high-frequency disturbances.

To understand whether the high energy non-zero frequencies are associated with a streamwise or spanwise travelling instability, the coherence between a fixed and traversing wire is plotted in Figure 9. In the absence of a strip, the plot shows strong coherence between the two wires when separated by a distance of $\frac{1}{2}\lambda_c$ for $f < 100$ Hz. This may correspond to the hotspots seen in fluctuating velocity brought about by variations in $\mathrm{d}U/\mathrm{d}z$. The two signals are also coherent for frequencies between 100 Hz – 300 Hz across wire separations of 10 mm – 16 mm. The coherence drops off for larger wire separations, and in part, is possibly due to the travelling crossflow wave angle not being equal to the wing sweep angle at which these measurements were performed. For $x_h/c = 0.03, 0.10$, the magnitude of coherence increases for $f < 100$ Hz; the larger coherence at higher frequencies is not high enough to draw any significant conclusions. For $x_h/c = 0.20$, the spanwise spacing of the low-frequency disturbances is reduced to $\frac{1}{4}\lambda_c$ and coherence is strong for $f < 50$ Hz; the coherence is increased at the critical wavelength for frequencies between 300 Hz – 2000 Hz.

CONCLUSION

Our two key conclusions are, first, that the response to the 2D strip exhibits the combined effects of isolated backward and forward facing steps, in which unsteadiness is introduced by the former, and amplification of the stationary crossflow is caused by the latter. The second is that, unlike the observations of Deyhle & Bippes (1996), 2D roughness does have an impact on the mean flow.

We are indebted to Airbus for providing the AERAST wing and to BMT Fluid Mechanics for use of their wind tunnel. We acknowledge the financial support through the LFC-UK grant, EPSRC, EP/I037946.

REFERENCES

Bippes, H. 1999 Basic experiments on transition in three-dimensional boundary layers dominated by crossflow instability. *Progress in Aerospace Sciences* pp. 363–412. doi: 10.1016/S0376042199000020.

Crawford, B. K., Duncan Jr, G. T., Tufts, M.W., Saric, W. S. & Reed, H.L. 2015 Effects of step-excrescence location on swept-wing transition. In *53rd AIAA Aerospace Sciences Meeting*, *AIAA* 2015-1233. doi: 10.2514/6.2015-1233.

Deyhle, H. & Bippes, H. 1996 Disturbance growth in an unstable three-dimensional boundary layer and its dependence on environmental conditions. *Journal of Fluid Mechanics* **316**, 73–113. doi: 10.1017/s0022112096000456.

Downs, R. S. 2012 Environmental influences on crossflow instability. PhD thesis, Texas A&M University.

Duncan Jr., G.T., Crawford, B.K., Tufts, M.W., Saric, W.S. & Reed, H.L. 2013 Effects of step excrescences on swept-wing transition. In *31st AIAA Applied Aerodynamics Conference, Fluid Dynamics and Co-located Conferences*, *Paper* 2013-2412. doi: 10.2514/6.2013-2412.

Duncan Jr, G. T., Crawford, B. K., Tufts, M.W., Saric, W. S. & Reed, H.L. 2014 Effects of step excrescences on a swept wing in a low-disturbance wind tunnel. In *AIAA SciTech Forum*, *AIAA* 2014-0910. doi: 10.2514/6.2014-0910.

Eppink, J.L. 2014 The interaction of crossflow instabilities and a backward facing step in swept boundary layer transition. PhD thesis, Tufts University.

Eppink, J.L., Wleizen, R.W., King, R.A. & Choudhari, M. 2018 Interaction of backward-facing step and crossflow instabilities in boundary-layer transition. *AIAA Journal* **56** (2), 497–509. doi: 10.2514/1.J056267.

Mughal, M. S. & Ashworth, R. 2013 Uncertainty quantification based receptivity modelling of crossflow instabilities induced by distributed surface roughness in swept wing boundary layers. In *43rd AIAA Fluid Dynamics Conference*, *AIAA* 2013-3106. doi: 10.2514/6.2013-3106.

Sunderland, R. & Sawyers, D. 2009 Evaluation of AERAST large scale wind-tunnel test results. *Tech. Rep.* RP0905747. Airbus.

Tufts, M.W., Reed, H.L., Crawford, B.K., Duncan, Jr., G.T. & Saric, W.S. 2017 Computational investigation of step excrescence sensitivity in a swept-wing boundary layer. *Journal of Aircraft* **54** (2), 602–626. doi: 10.2514/1.C033892.

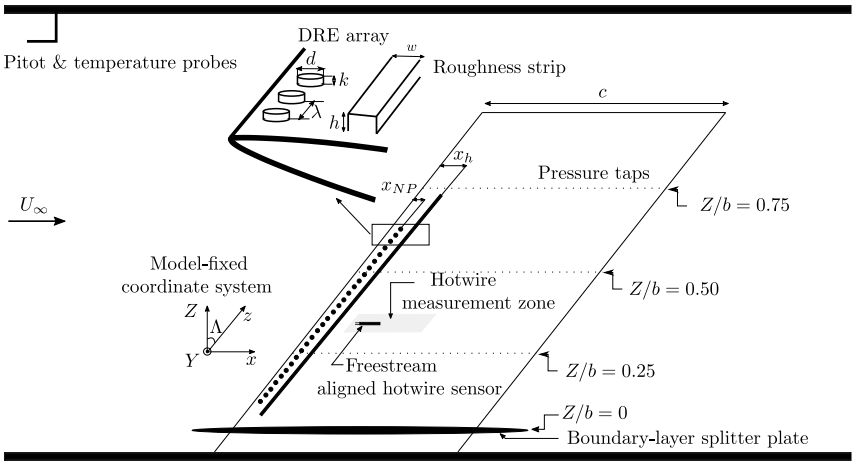

Figure 1: Side view of experimental setup.

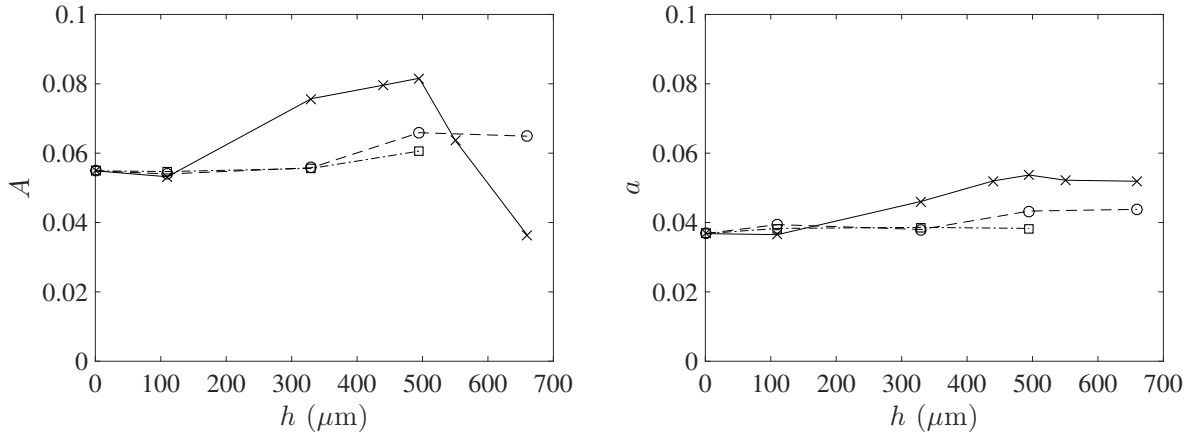

Figure 2: Disturbance amplitude variation with strip height and chordwise location measured at $x/c = 0.25$, $k = 44$ μm: (a) stationary disturbances; (b) travelling disturbances. Symbols (×, □, ○) represent measurements at $x_h/c = 0.03, 0.10, 0.20$.

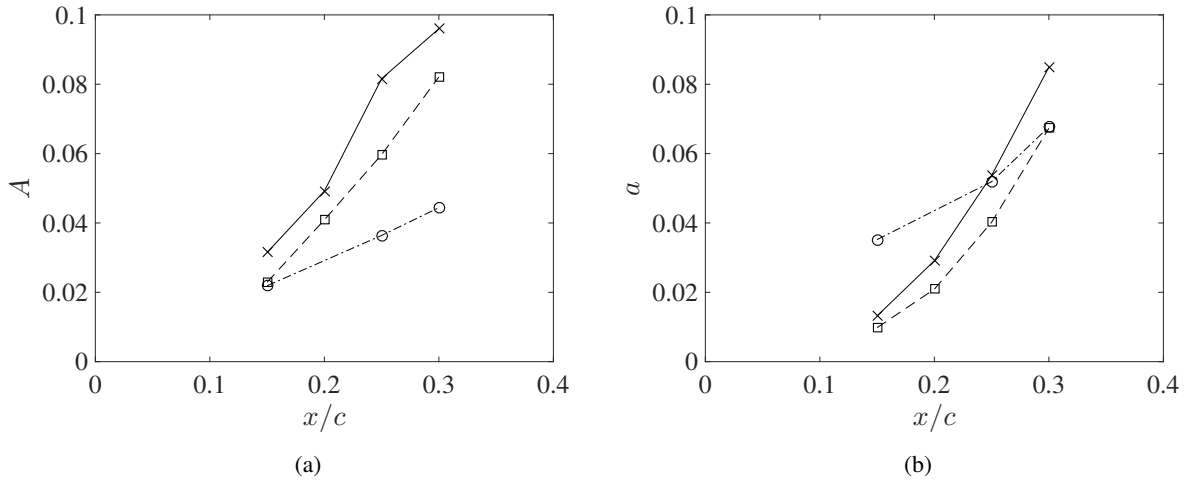

Figure 3: Disturbance amplitude, streamwise evolution: (a) stationary wave and (b) travelling wave, at $x_h/c = 0.03$, $k = 44$ μm. Symbols (□, ×, ○) represent measurements with strip at $h = (0, 495, 660)$ μm.

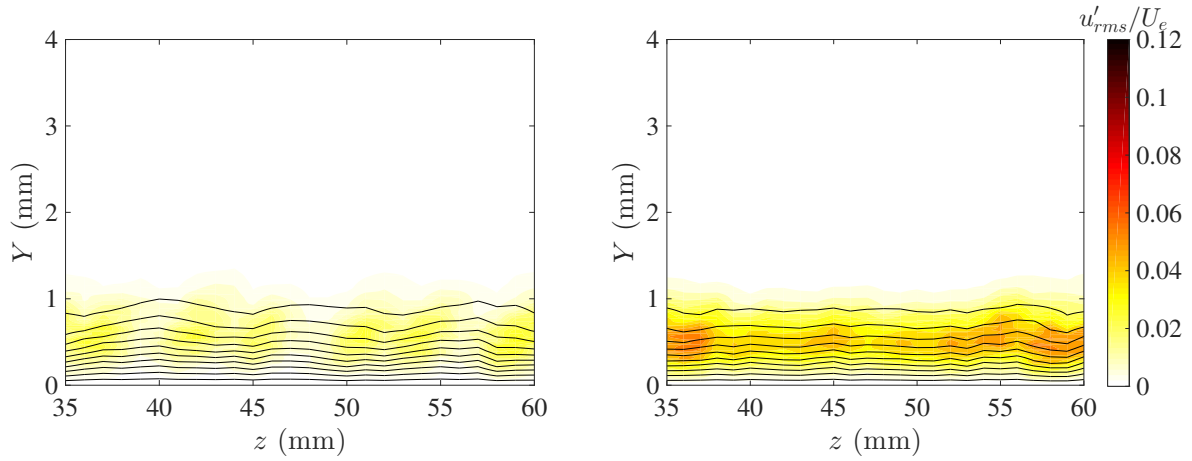

Figure 4: Contours of U (black lines) and u'_{rms} (colour map) measured at $x/c = 0.15$, $x_h/c = 0.03$, $k = 44$ μm: (a) $h = 495$ μm; (b) $h = 660$ μm.

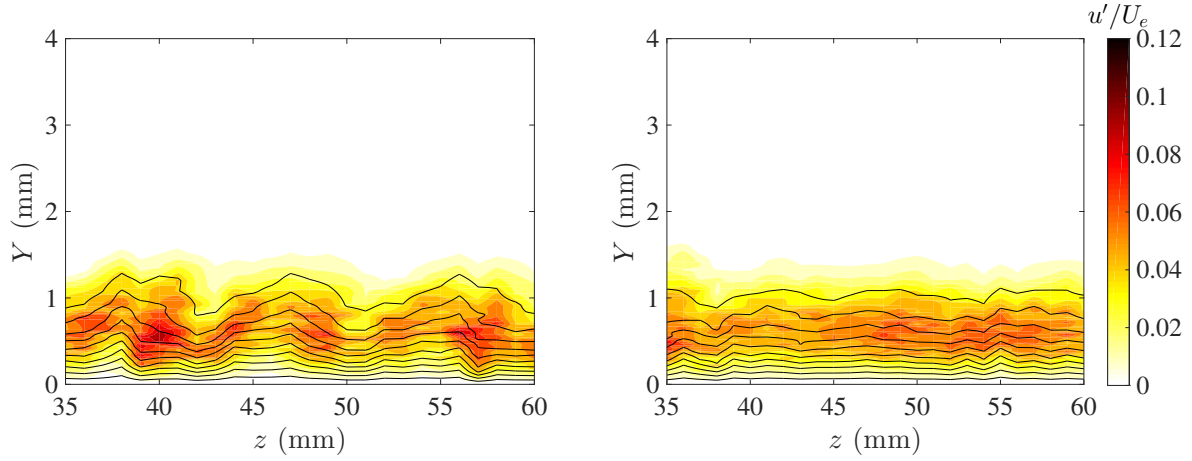

Figure 5: Contours of U (black lines) and u'_{rms} (colour map) measured at $x/c = 0.25$, $x_h/c = 0.03$, $k = 44$ μm: (a) $h = 495$ μm; (b) $h = 660$ μm.

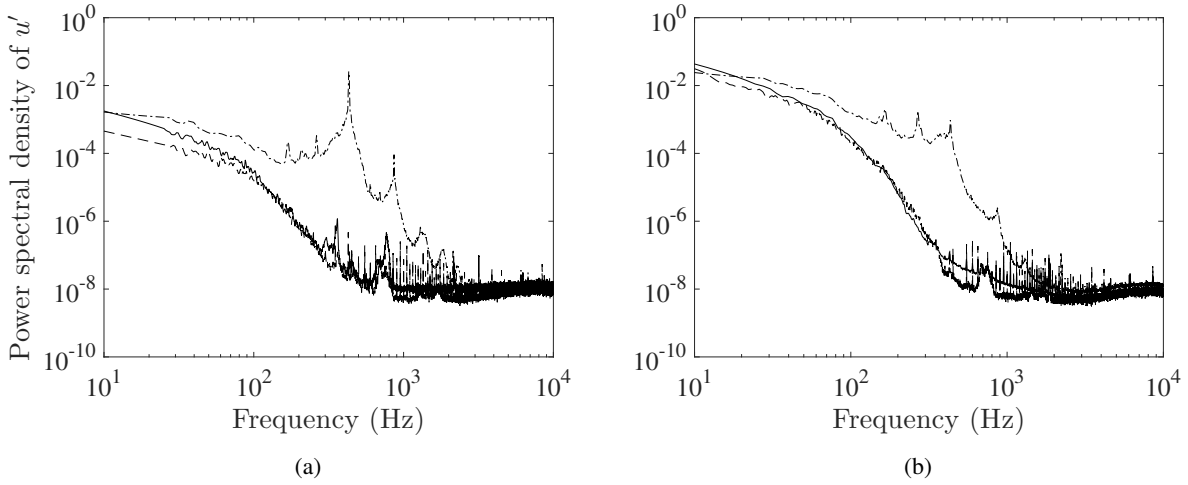

Figure 6: Power spectral densities of u' measured at $x_h/c = 0.03$, $k = 44$ μm: (a) $x/c = 0.15$, $Y \approx 0.50$ mm, $z = 44$ mm; (b) $x/c = 0.25$, $Y \approx 0.71$ mm, $z = 48$ mm. Lines (- - -,——, - · - ·) represent measurements at $h = (0, 495, 660)$ μm.

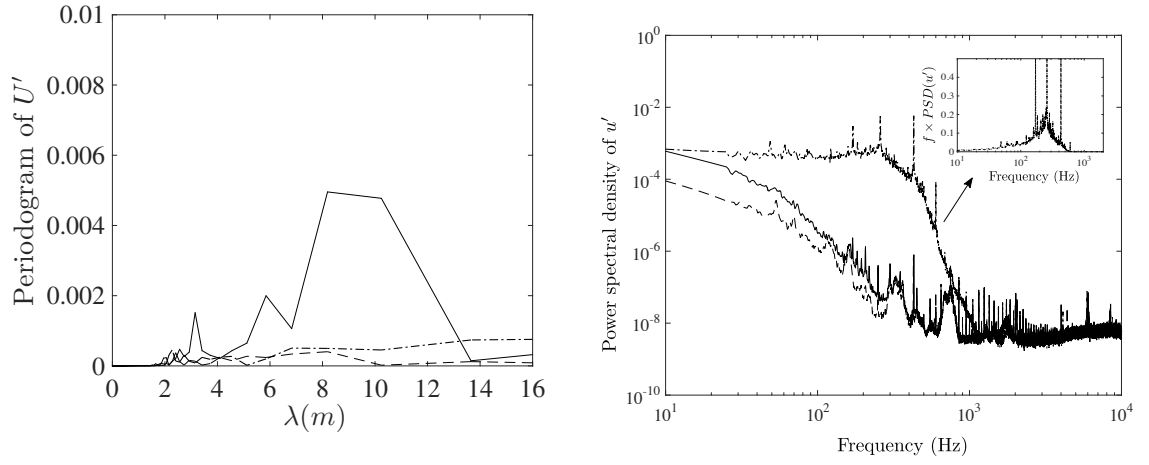

(a) (b)

Figure 7: Power spectral densities measured at $x/c = 0.25$, $x_h/c = 0.03$, clean leading edge: (a) spanwise distribution of stationary disturbances; (b) unsteady velocity u' at $Y \approx 0.50$ mm, $z = 48$ mm. (- - -, ——, - · - ·) represent measurements at $h = (0, 495, 660)$ μm.

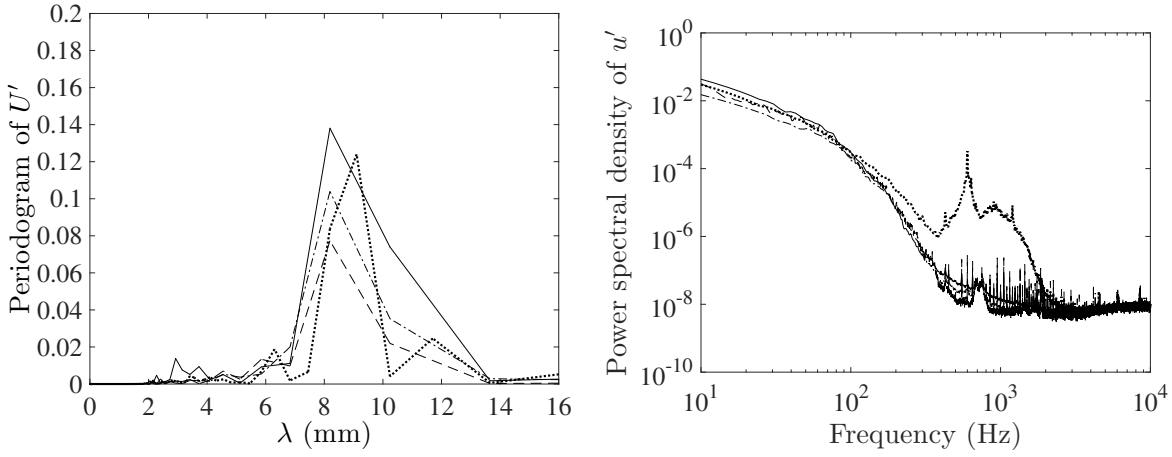

(a) (b)

Figure 8: Power spectral densities measured at $x/c = 0.25$, $h = 495$ μm, $k = 44$ μm: (a) spanwise distribution of stationary disturbances; (b) unsteady velocity u' at $Y \approx 0.71$ mm, $z = 48$ mm. Lines (- - -, ——, - · - ·, ·····) represent measurements at $x_h =$ no strip, 0.03, 0.10, 0.20.

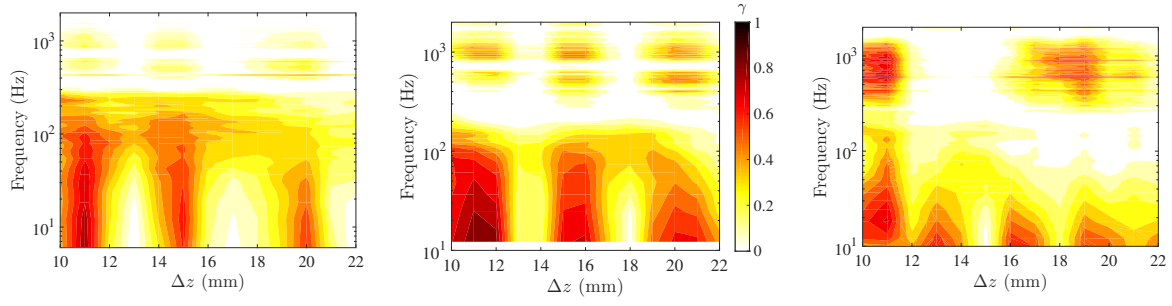

(a) (b) (c)

Figure 9: Coherence (colour map) between traverse and fixed probe at multiple spanwise locations measured at $x/c = 0.25$, $h = 495$ μm, $k = 44$ μm, $Y \approx 0.71$ mm: (a) no strip, (b) $x_h/c = 0.03$, (c) $x_h/c = 0.20$.